HMG Advance Access published November 30, 2010

Human Molecular Genetics, 2010 **1–11**
doi:10.1093/hmg/ddq492

Glycogen-branching enzyme deficiency leads to abnormal cardiac development: novel insights into glycogen storage disease IV

Yi-Ching Lee[1,2], Chia-Jung Chang[1], Deeksha Bali[3], Yuan-Tsong Chen[1,4] and Yu-Ting Yan[1,*]

[1]Institute of Biomedical Sciences, Academia Sinica, Taipei 11529, Taiwan, [2]Graduate Institute of Integrated Medicine, China Medical University, Taichung 404, Taiwan, [3]Division of Medical Genetics, Department of Pediatrics, Duke University Medical Center, Durham, NC 27710, USA and [4]Department of Pediatrics, Duke University Medical Center, Durham, NC 27710, USA

Received July 20, 2010; Revised and Accepted November 5, 2010

Glycogen storage disease type IV (GSD-IV) is an autosomal recessive disease caused by a deficiency in glycogen-branching enzyme (GBE1) activity that results in the accumulation of amylopectin-like polysaccharide, which presumably leads to osmotic swelling and cell death. This disease is extremely heterogeneous in terms of tissue involvement, age of onset and clinical manifestation. The most severe fetal form presents as hydrops fetalis; however, its pathogenetic mechanisms are largely unknown. In this study, mice carrying a stop codon mutation (E609X) in the *Gbe1* gene were generated using a gene-driven mutagenesis approach. Homozygous mutants (*Gbe*$^{-/-}$ mice) recapitulated the clinical features of hydrops fetalis and the embryonic lethality of the severe fetal form of GSD-IV. However, contrary to conventional expectations, little amylopectin accumulation and no cell degeneration were found in *Gbe*$^{-/-}$ embryonic tissues. Glycogen accumulation was reduced in developing hearts of *Gbe*$^{-/-}$embryos, and abnormal cardiac development, including hypertrabeculation and noncompaction of the ventricular wall, was observed. Further, *Gbe1* ablation led to poor ventricular function in late gestation and ultimately caused heart failure, fetal hydrops and embryonic lethality. We also found that the cell-cycle regulators cyclin D1 and c-Myc were highly expressed in cardiomyocytes and likely contributed to cardiomyocyte proliferation and trabeculation/compaction of the ventricular wall. Our results reveal that early molecular events associated with Gbe1 deficiency contribute to abnormal cardiac development and fetal hydrops in the fetal form of GSD-IV.

INTRODUCTION

Glycogen storage disease type IV (GSD-IV; OMIM232500), also known as Andersen disease, is an autosomal recessive genetic disorder that results from a deficiency in the activity of the glycogen-branching enzyme GBE1, an amylo-(1,4-1,6)-transglycosylase (EC 2.4.1.18). The glycogen-branching enzyme adds short glucosyl chains in α-1,6 glycosidic links to the glycogen molecule to yield a branched polymer with increased water solubility and glycogen synthetic activity. A deficiency of this enzyme results in tissue accumulation of abnormal glycogen with fewer branch points and longer outer branches that resembles an amylopectin-like structure, also known as polyglucosan. This structurally abnormal glycogen has low solubility and forms precipitates in the liver, heart and muscle (1–3).

GSD-IV is a clinically heterogeneous disorder. Since the original description of the classical progressive hepatic form of GBE deficiency by Andersen in 1952, many variants of GSD-IV with different tissue involvement and variable clinical manifestations have been observed. The age of onset ranges from fetus to adulthood and is divided into four groups: (i) perinatal, presenting as fetal akinesia deformation sequence and perinatal death (4,5); (ii) congenital, with hydrops fetalis, neuronal involvement and death in early infancy (6–8); (iii) childhood, with myopathy or

*To whom correspondence should be addressed at: Institute of Biomedical Sciences, Academia Sinica, 128 Academia Road, Section 2, Nankang, Taipei 11529, Taiwan. Tel: +886 226523941; Fax: +886 227827654; Email: yyan@ibms.sinica.edu.tw

cardiomyopathy (9,10); and (iv) adult, with isolated myopathy or adult polyglucosan body disease (11,12).

Despite the fact that this disease has been known for many years, questions concerning its pathogenesis and molecular mechanisms have remained unanswered. It has been suggested that accumulation of the less soluble abnormal polysaccharide causes a foreign body reaction in the cell, leading to osmotic swelling and cell death (1). Mutations identified in patients reveal that the different forms of GSD-IV are caused by different mutations in the same gene, with severe mutations causing more severe phenotypes (13). Further studies are needed to understand the underlying molecular mechanisms of the various presentations of GSD-IV.

Although GBE1 deficiency has been reported in horses and cats (14,15), there has been no mouse model for GSD-IV. Here, we report the generation of a GSD-IV mouse model carrying a stop mutation (E609X) in the *Gbe1* gene using a gene-driven ENU (*N*-ethyl-*N*-nitrosourea)-mutagenesis approach. The GSD-IV $Gbe^{-/-}$ mice exhibited hydrops fetalis and lethality between mid and late gestation, recapitulating the clinical features of severe fetal neuromuscular forms of human GSD-IV. Contrary to conventional expectations, $Gbe^{-/-}$ embryos exhibited less glycogen accumulation than their wild-type (WT) littermates. The morphological abnormalities of embryonic $Gbe^{-/-}$ hearts and underlying mechanisms were identified.

RESULTS

Generation of mice carrying *Gbe1* mutations

Both mouse and human GBE1 are 702-amino-acid proteins encoded by 16 exons; their amino acid sequences share 95% similarity and 91% identity (Supplementary Material, Fig. S1). To isolate appropriately mutated *Gbe1* clones, we screened an ENU-mutagenized mouse DNA archive, focussing on *Gbe1* exons 5, 7, 12 and 14, which contain longer amino acid coding sequence and more identified mutations associated with GSD-IV in humans (Supplementary Material, Fig. S1). As shown in Supplementary Material, Figure S1 and Table S1, these screens revealed one nonsense mutation (E609X), six missense mutations (M302L, H319Q, Y329F, M522K, H608Q and G609R), three silent mutations (A214A, L506L and G532G) and three intronic mutations (intron 5, intron 7 and intron 11). Several nonsense and splice site mutations led to prematurely truncated Gbe1 proteins, which are known to cause the severe perinatal/congenital neuromuscular forms of GSD-IV in humans (1,16). Therefore, we established a mouse line in a C3HeB/FeJ background using the E609X mutant—a G-to-T nonsense mutation located within exon 14 that created a stop codon at amino acid position 609. No obvious phenotypes were observed in heterozygous $Gbe^{+/-}$ mice. Second-generation heterozygous mice were outcrossed to WT C3HeB/FeJ mice for two more generations to dilute potential unrelated mutations. Fourth-generation $Gbe^{+/-}$ pairs, which shared an estimated 1.25 common mutations (17), were then intercrossed to generate homozygous $Gbe^{-/-}$ mice.

Perinatal mortality of homozygous E609X mice

No live-born $Gbe^{-/-}$ mice were recovered (Table 1). To investigate the timing of *in utero* $Gbe^{-/-}$ lethality, we performed timed matings of $Gbe^{+/-}$ mice and examined embryos on embryonic days 10.5 (E10.5) to term by high-frequency ultrasound biomicroscopy. Embryonic survival was determined on the basis of the observation of beating hearts. The survival rate of $Gbe^{-/-}$ embryos decreased with increasing stage of embryonic development; at E10.5, survival was 67%, and decreased to 57% at E12.5–E15.5, 36% at E16.5–E19.5 and 0% at term (Table 1). The latest survivors were observed at E17.5. We conclude that $Gbe^{-/-}$ embryos died predominantly at mid-to-late gestational stages.

Decreased heart rate and diminished accumulation of glycogen in mid-gestation $Gbe^{-/-}$ embryos

Heart rates in developing $Gbe^{-/-}$ embryos (30–65 b.p.m.) were markedly decreased compared with those of their WT littermates (114–121 b.p.m.) at E10.5 (Fig. 1A). To explore the causes of slow heart rate and embryonic lethality of $Gbe^{-/-}$ mice in greater detail, we first examined glycogen accumulation in the developing embryos by periodic acid-Schiff (PAS) staining. At E10.5, there was a major accumulation of glycogen in the ventricular and atrial chamber wall of the developing hearts of WT embryos (Fig. 1Bc and e), but no glycogen staining was detected in the heart chamber of $Gbe^{-/-}$ embryos (Fig. 1Bd and f). Significantly lower levels of glycogen staining were also evident in the hearts of $Gbe^{-/-}$ embryos at subsequent developmental stages E14.5 (Fig. 2; compare b and d, and a and c in A) and E16.5 (Fig. 2; compare b and d, and a and c in B). The glycogen levels in the hearts of E16.5 WT and $Gbe^{-/-}$ embryos were further analyzed. The glycogen levels in the hearts of E16.5 $Gbe^{-/-}$ embryos were found to be significantly lower compared with those in WT embryos (Fig. 2C). At E11.5, glycogen also accumulated in the main bronchus of the lung bud in WT embryos (Supplementary Material, Fig. S2A) and could be detected in hepatic primordium in WT and $Gbe^{-/-}$ embryos (Supplementary Material, Fig. S2A–D). Glycogen accumulation in the liver and skeletal muscle was not significantly different between $Gbe^{-/-}$ and WT embryos at late gestational stages (Supplementary Material, Fig. S2; compare E and F, and I and J). We further tested for abnormal glycogen accumulation in the hearts, liver and skeletal muscle of $Gbe^{-/-}$ embryos by pretreating the tissue with diastase before PAS staining. No PAS-positive, diastase-resistant deposits were detected in the hearts of E11.5 or E12.5 $Gbe^{-/-}$ embryos (Supplementary Material, Fig. S3). Small amounts of PAS-positive, diastase-resistant material were observed in the hearts at E14.5 (Fig. 2; compare h and g in A) and E16.5 (Fig. 2; compare h and g in B), in the liver at E14.5 and in the skeletal muscle of stillborn $Gbe^{-/-}$ embryos (Supplementary Material, Fig. S2; compare G and H, and K and L), but no obvious cell disruption or structure defects were observed.

To determine whether the lower level of glycogen in the hearts of $Gbe^{-/-}$ embryos was directly correlated with *Gbe1* expression, we measured *Gbe1* transcripts in the hearts

Table 1. Survival of mutant embryos

Age	WT	$Gbe^{+/-}$	$Gbe^{-/-}$	Survival rate[a]	Total
E10.5	22 (1)[b]	34 (1)	15 (5)	67%	71
E12.5–15.5	7 (0)	16 (0)	7 (3)	57%	30
E16.5–19.5	13 (0)	17 (1)	11 (7)	36%	41
Newborn	11 (1)	19 (0)	15 (15)	0	45
Total	53	86	48		187

Shown are embryos obtained from timed heterozygous matings. The numbers of embryos of each genotype obtained at the indicated time are listed. The numbers in the last column are the total number of embryos collected at each gestational age. The numbers in the last row indicate the total number of embryos of each genotype collected.
[a]The survival rate of $Gbe^{-/-}$ mice at each gestational age.
[b]Parenthetic values indicate embryos without a detectable heart beat, determined by ultrasound microscopy.

from different embryonic stages by real-time reverse transcription-polymerase chain reaction (RT-PCR) using primers designed against three specific regions of *Gbe1* cDNA. Gbe1 mRNA levels were significantly reduced in the hearts of $Gbe^{-/-}$ embryos compared with WT embryos at all developmental stages tested (Fig. 1C). These results suggest that the stop codon mutation in the *Gbe1* gene compromises *Gbe1* transcription, affecting Gbe1 protein level and glycogen synthesis in the developing heart, and ultimately leading to the lethality of $Gbe^{-/-}$ embryos.

Heart defects in Gbe1-deficient embryos

Our examination of embryos for gross abnormalities revealed a congested venous system in the peripheral vasculature and generalized edema in E14.5 $Gbe^{-/-}$ embryos (Fig. 3; compare A and B). A further analysis of organ sections from E14.5 $Gbe^{-/-}$ embryos showed a congested venous system in the lung (Fig. 3; compare G and H) and liver (Fig. 3; compare I and J). At E15.5, prominent livers were also evident in $Gbe^{-/-}$ embryos in addition to edema (Fig. 3; compare C and D). The hearts of stillborn $Gbe^{-/-}$ mice showed significantly smaller ventricles compared with those from newborn WT mice and, in most cases, had extensive pooling of blood (Fig. 3; compare E and F). These results suggest that poor functioning hearts in mid-to-late gestation $Gbe^{-/-}$ embryos contributed to embryonic lethality.

Next, we analyzed serial histological sections of $Gbe^{-/-}$ and WT embryonic hearts from E11.5 to term to determine whether abnormalities in cardiac development might have contributed to poor heart function and embryonic lethality. The $Gbe^{-/-}$ hearts displayed the expected pattern of heart looping, cardiac outflow tract septation and cardiac chamber segmentation at E11.5 (Fig. 4; compare A and B). However, at E12.5, the hearts of $Gbe^{-/-}$ embryos exhibited reduced ventricular compaction and a thinner compact myocardium zone than those of WT embryos (Fig. 4; compare C and D, E and F). At E13.5, in addition to the reduced ventricular compaction and a thinner compact myocardium zone (Fig. 4; compare G and H), the interventricular septa of $Gbe^{-/-}$ embryos were thinner and had a looser structure than those of WT hearts (Fig. 4; compare G and H); these differences were also evident at E14.5 (Fig. 4; compare I and J). At E15.5 and E16.5, the ventricular cavities of $Gbe^{-/-}$ embryonic hearts were smaller than those of WT hearts and, unlike those of WT hearts, were nearly filled with cells (Fig. 4; compare K and L, and M and N). Frank ventricular septum defects (VSD) were observed in some stillborn $Gbe^{-/-}$ mice (Fig. 4; compare O and P). These results suggest that abnormalities in heart development contribute to embryonic lethality in $Gbe^{-/-}$ embryos.

Cardiomyocyte hyperproliferation accounts for the hypertrabeculation and ventricular noncompaction in $Gbe^{-/-}$ hearts

To identify the cells that occupied the nearly filled ventricular cavities of late-gestation (E16.5) $Gbe^{-/-}$ hearts, we performed immunofluorescence staining. Using the myocardial marker MF-20, we confirmed that these cells were cardiomyocytes (Fig. 5A). Confocal microscopy revealed long trabecular projections and a thin compact zone with no significant Z-line/body or organized sarcomeres in E16.5 $Gbe^{-/-}$ hearts (Fig. 5A and B), suggesting extensive trabecula and nonmaturation/noncompaction of the compact wall in $Gbe^{-/-}$ hearts. To address the possibility that this phenotype might be secondary to increased proliferation of cardiomyocytes at an earlier stage, we stained heart sections for phosphorylated histone H3, an M-phase-specific marker, and found a marked increase in the number of positive-stained cells in the ventricular wall area of E14.5 $Gbe^{-/-}$ hearts (Fig. 5C). These observations suggest that the cell-filled ventricles observed in late-gestation $Gbe^{-/-}$ hearts result from hypertrabeculation caused by altered regulation of cell proliferation and maturation during ventricular wall formation, which, in turn, led to a decrease in ventricular wall compaction. Therefore, the heart failure observed in $Gbe^{-/-}$ embryos is the result of hyperproliferation of cardiomyocytes and subsequent hypertrabeculation/noncompaction.

Gbe1-deficiency alters the expression of cell-cycle regulators

To explore the mechanism by which Gbe1 deficiency might affect cardiac trabeculation and/or compaction, we first analyzed bone morphogenetic protein 10 (Bmp10). Bmp10, a peptide growth factor that belongs to the TGF-β superfamily, has been suggested to be a key morphogenetic growth factor in the regulation of cardiac trabeculation and/or compaction (18,19). *Bmp10* transcript levels decreased in the developing heart during late gestational stages (Supplementary Material, Fig. S4), as described previously (19). However, no significant differences in *Bmp10* transcript levels were observed in the hearts of $Gbe^{-/-}$ and WT embryos at E14.5 or at term (Supplementary Material, Fig. S4). We further analyzed cyclin D1 and c-Myc, the cell-cycle regulators, which have been shown to drive cardiomyocyte proliferation (20). Cyclin D1 expression levels were increased in $Gbe^{-/-}$ hearts compared with WT hearts (Fig. 6A and B). An analysis of c-Myc levels in heart sections of $Gbe^{-/-}$ and WT showed that c-Myc was highly expressed in the cardiomyocytes of $Gbe^{-/-}$ embryos, but was expressed in only a small restricted area of

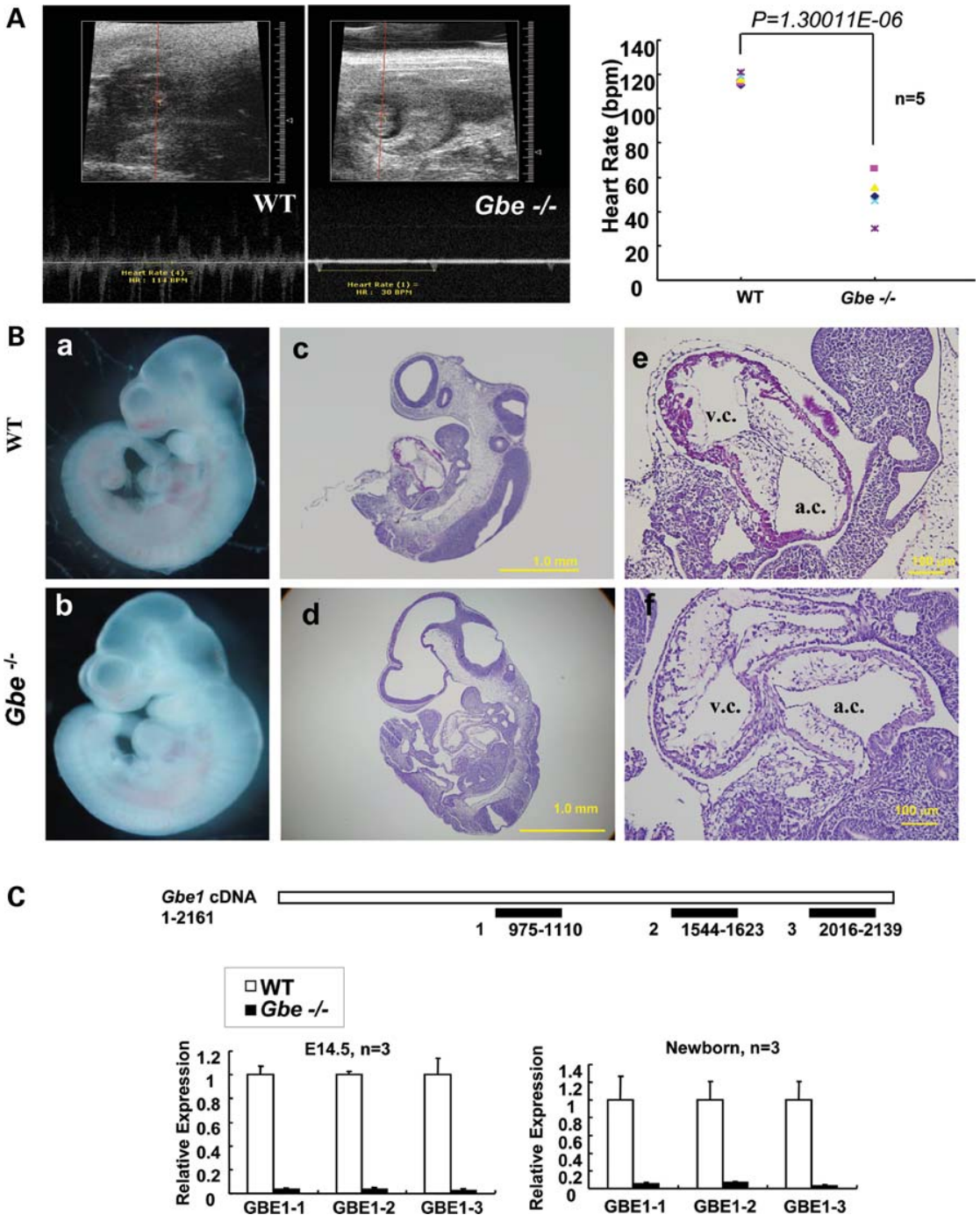

Figure 1. Heart rate, morphology, glycogen accumulation and *Gbe1* expression in E10.5 WT and $Gbe^{-/-}$ embryos. (**A**) E10.5 WT and $Gbe^{-/-}$ embryo echocardiograms (left panel) and heart rates (right panel). Heart rates in E10.5 $Gbe^{-/-}$ embryos were slower than those in E10.5 WT embryos ($P < 0.001$; $n = 5$ embryos each for $Gbe^{-/-}$ and WT, both from the same three pregnant mothers). (**B**) Morphological and histological analyses of E10.5 embryos. Both WT (a) and $Gbe^{-/-}$ (b) embryos exhibited normal morphological development. PAS staining of sections from E10.5 embryos showed substantial glycogen accumulation in the developing heart chamber wall in E10.5 WT embryos (c and e), but no glycogen accumulation in $Gbe^{-/-}$ embryos (d and f). v.c., ventricular chamber; a.c., atrial chamber. (**C**) Relative Gbe1 mRNA levels in the hearts of WT and $Gbe^{-/-}$ mice at E14.5 and newborns (WT)/stillborns ($Gbe^{-/-}$) analyzed by real-time RT-PCR ($n = 3$).

the ventricular trabecular myocardium in WT hearts (Fig. 6C). These results suggest that the dysregulation of cell-cycle regulators, cyclin D1 and c-Myc, might contribute to hyperproliferation of cardiomyocytes and subsequent hypertrabeculation/noncompaction of the ventricular wall in $Gbe^{-/-}$ embryos.

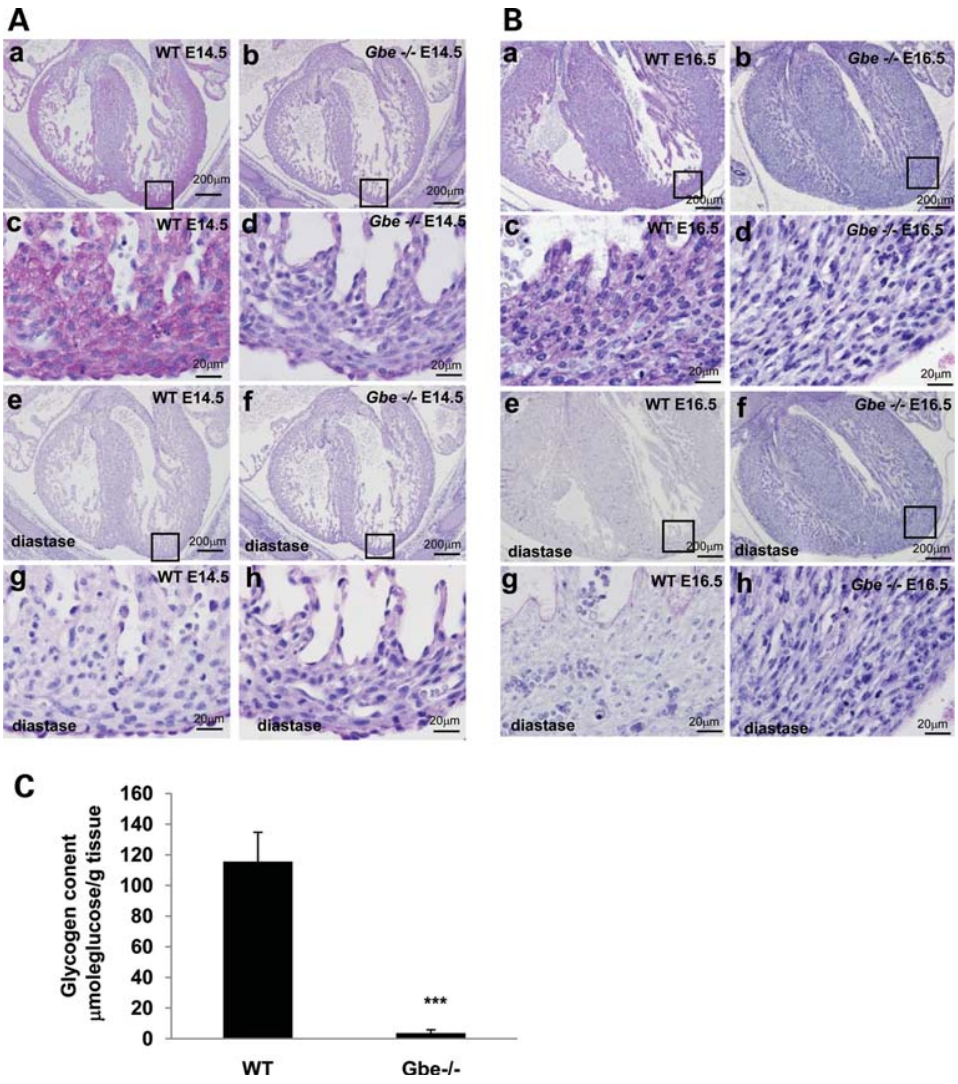

Figure 2. Glycogen accumulation in the hearts of E14.5 and E16.5 embryos from $Gbe^{-/-}$ and WT mice. Heart sections of $Gbe^{-/-}$ embryos showed less PAS-positive staining (glycogen accumulation) than those from WT embryos at E14.5 (**A**) and E16.5 (**B**). Only a small amount of diastase-resistant PAS-positive staining (abnormal glycogen) was detected in the hearts of E14.5 and E16.5 $Gbe^{-/-}$ embryos. Scale bars: 200 μm (a, b, e and f) and 20 μm (c, d, g and h). Diastase: PAS staining after diastase incubation. (**C**) Glycogen content was determined in the hearts of E16.5 WT and $Gbe^{-/-}$ embryos ($n = 3$ biological samples, $P < 0.001$).

DISCUSSION

Herein we describe the first mouse model of GSD-IV disease. This $Gbe^{-/-}$ mouse model recapitulates the clinical features of hydrops fetalis and the embryonic lethality of severe fetal neuromuscular forms of human GSD-IV. Using it, we identify the underlying mechanisms that lead to hydrops fetalis. The deficiency of Gbe1 led to reduced glycogen accumulation in developing hearts. Furthermore, our studies found that expression of cyclin D1 and c-Myc, two factors which have a role in cardiomyocyte proliferation during heart development, was increased in $Gbe^{-/-}$ embryos. The hyperproliferation of cardiomyocytes impaired trabeculation/compaction of ventricular wall, leading to poor ventricular function in late gestation and, ultimately, to heart failure, fetal hydrops and embryonic lethality.

The fetal and infantile forms of GSD-IV are relatively rare. A complete absence of GBE1 enzyme activity results in the development of fetal hydrops and akinesia during the second trimester. Brain examinations of affected fetuses have shown intraventricular hemorrhage. Diastase-resistant amylopectin accumulates exclusively in fetal skeletal muscle cells and the heart, but not in the liver or neurons (5,21). However, the mechanisms responsible for human GSD-IV fetal hydrops and akinesia have remained unclear; notably, the structure and function of fetal hearts have not been examined in detail. Our findings based on the $Gbe^{-/-}$ mouse model suggest that morphological and functional abnormalities of fetal hearts might be the underlying cause of fetal hydrops. Several cases of perinatal neuromuscular forms of GSD-IV have been reported by different groups (7,16,21,22). Severe hypotonia and dilated cardiomyopathy (which were attributed

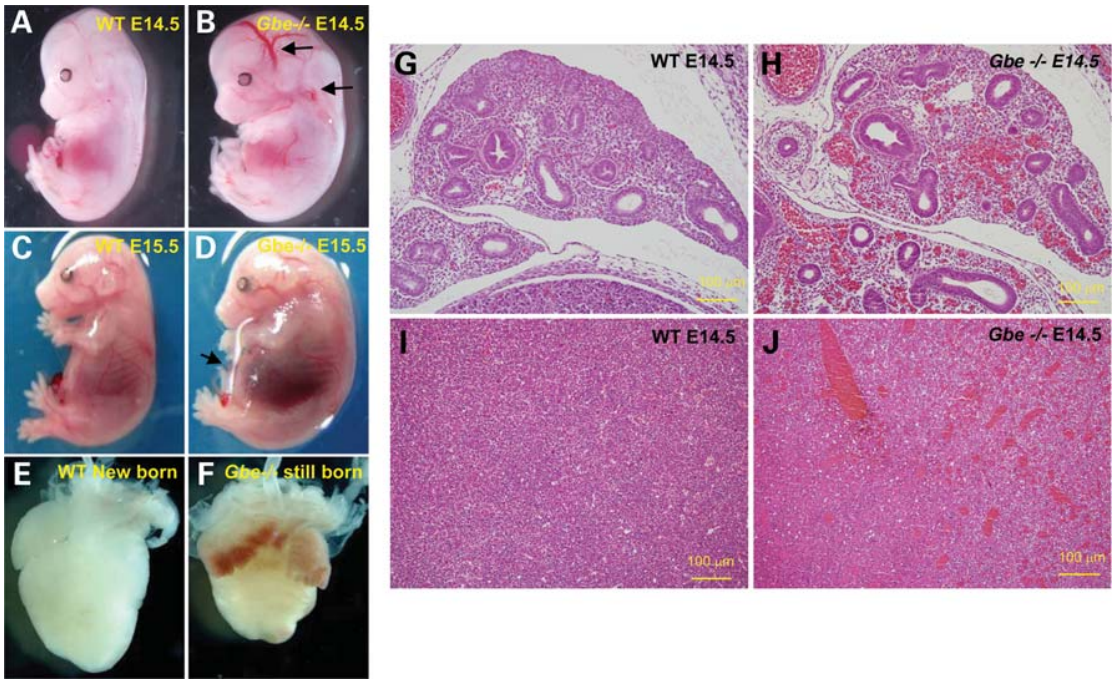

Figure 3. Blood congestion in $Gbe^{-/-}$ embryos. Morphological (**A**–**F**) and histological (**G**–**J**) examination of blood distribution in WT and $Gbe^{-/-}$ embryos. A morphological examination of E14.5 embryos showed congested vessels (indicated by arrows) and edema in $Gbe^{-/-}$ mice (B) compared with WT mice (A). At E15.5, $Gbe^{-/-}$ embryos exhibited prominent liver (D; indicated by arrow) in addition to edema (compare with WT mice in C). The hearts from stillborn $Gbe^{-/-}$ mice (F) showed smaller ventricles and congested blood in atria compared with those from WT newborns (E). H&E-stained sections of E14.5 $Gbe^{-/-}$ embryos (H) showed evidence of blood congestion in the pulmonary parenchyma (compare with WT embryos in G). H&E staining showed a similar degree of blood congestion in liver sections of E14.5 $Gbe^{-/-}$ (J) and WT (I) embryos. Scale bars: 100 μm (G–J).

to amylopectin deposits in cardiomyocytes) with subsequent extensive injury of myocardial fibers leading to heart failure were observed in these cases (7). In our $Gbe^{-/-}$ mouse model, fetal hydrops was observed, but little diastase-resistant amylopectin deposition was detected in the heart and no myocardial cell injury was observed. Therefore, this model allowed us to investigate the early molecular events involved in the pathogenesis of fetal-type GSD-IV before cell death occurred.

Glycogen occupies ∼2% of the cell volume in adult cardiac myocytes and >30% of the cell volume in fetal cardiac myocytes (23). Cardiac glycogen is present at high levels during early-to-mid gestation before falling to low levels at the time of birth (24–26), suggesting that glycogen might have a specific role in heart function and development. However, the physiologic role of glycogen in the fetal heart is still not completely understood. It has been shown that glycogen plays an important role as an energy source for developing cardiac myocytes, allowing them to proliferate and function to support adequate circulation for the developing embryo (27). In the present work, glycogen, which was highly accumulated in cardiomyocytes of E10.5 WT mice, was undetectable in cardiomyocytes of E10.5 $Gbe^{-/-}$ mice, and remained significantly lower during mid-to-late gestation stages (to newborn/stillborn) compared with WT mice. Heart rate was significantly decreased in E10.5 $Gbe^{-/-}$ mice compared with that in WT mice, and hyperproliferation of cardiomyocytes and hypertrabeculation/noncompaction of the ventricular wall were observed in late-gestation $Gbe^{-/-}$ embryos. These results suggest that, in addition to serving as an energy reserve, cardiac glycogen might also play a critical role in regulating normal heart development and maturation. A mouse model in which the ability to store glycogen in skeletal muscle and cardiac muscle was eliminated by disruption of the glycogen synthase 1 gene (*Gys1*) as reported previously (28). In these mice, glycogen was undetectable in cardiac muscle, and thin ventricular walls and reduced trabecular structures, attributable to a decrease in cell proliferation, were observed. Most *Gys1*-null animals died soon after birth due to impaired cardiac function, but ∼10% survived (27). Although glycogen was low in both *Gys1*-null and our $Gbe^{-/-}$ mouse models, the phenotypes of impaired heart development were quite different. These results imply that the abnormal heart development observed in $Gbe^{-/-}$ embryos is not simply due to insufficient glycogen-based energy to maintain normal cardiomyocyte growth, and suggest that glycogen homeostasis might play a critical role in regulating heart development and maturation.

$Gbe^{-/-}$ mice exhibited hypertrabeculation and a lack of ventricular wall compaction, which led to nearly filled ventricular cavities, poor heart function and, ultimately, heart failure—the major cause of embryonic lethality at late gestational stages. Ventricular trabeculation is one of the most critical steps of ventricular chamber development. The trabecular myocardium of embryonic mouse hearts rapidly expands during E9.5–E13.5, followed by maturation, a slowing of the cell-cycling rate, and compaction to form a thicker, compact ventricular wall after E14.5. The balance between proliferation and maturation is critical to the formation of

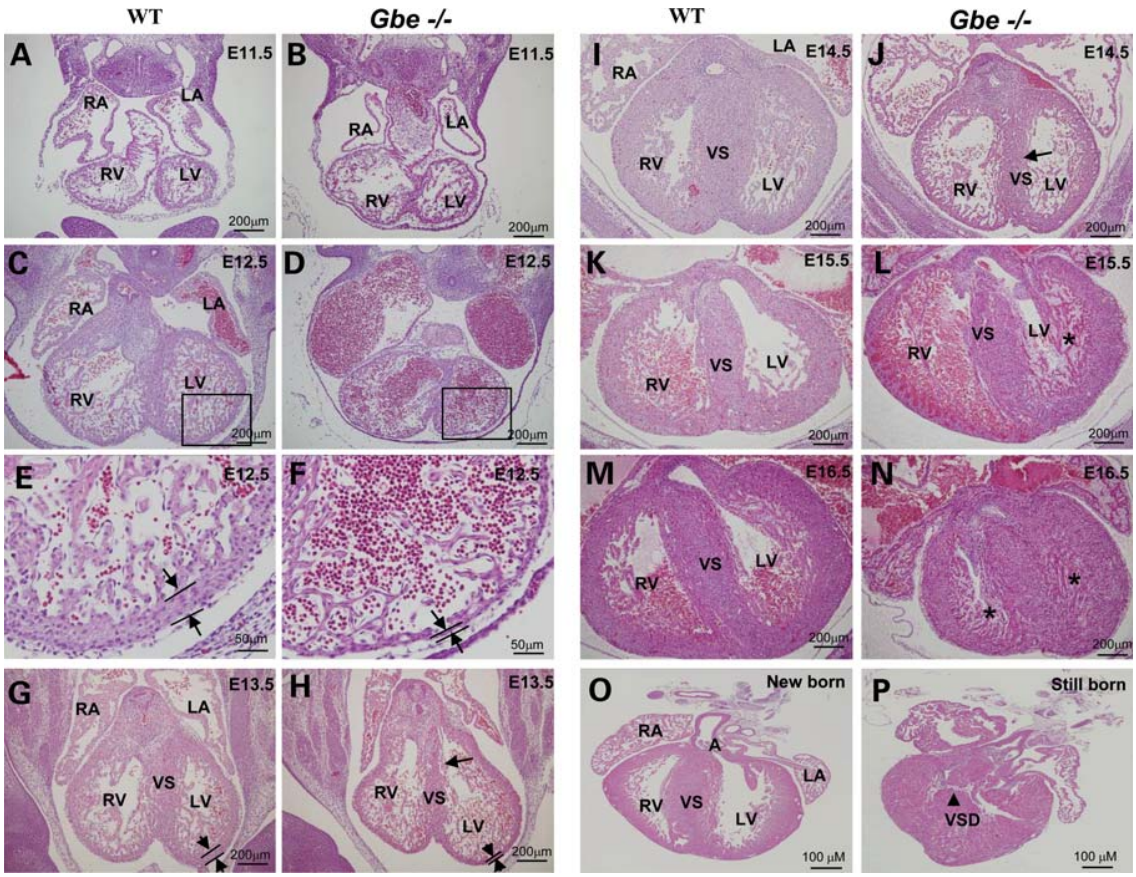

Figure 4. Histological analysis of heart development. Comparison of cardiac histology of $Gbe^{-/-}$ and WT at E11.5 (**A** and **B**), E12.5 (**C**–**F**), E13.5 (**G** and **H**), E14.5 (**I** and **J**), E15.5 (**K** and **L**), E16.5 (**M** and **N**) and in newborn/stillborn (**O** and **P**) mice. Images in (E) and (F) are higher magnifications of areas demarcated in (C) and (D), respectively. Arrows point to the thin compact myocardial zone of the ventricular wall in $Gbe^{-/-}$ embryonic hearts at E12.5 and E13.5 (F and H), the thin and loose interventricular septum in $Gbe^{-/-}$ embryonic hearts at E13.5 (H) and E14.5 (J) and VSD in stillborn $Gbe^{-/-}$ hearts (P). Asterisk denotes the filled ventricle at E15.5 (L) and E16.5 (N). RA, right atrium; LA, left atrium; RA, right ventricle; LA, left ventricle; VS, ventricular septum; VSD, ventricular septum defects.

a functionally competent ventricular wall. To identify mechanisms by which the lack of Gbe1 might lead to hypertrabeculation/noncompaction of the ventricular wall, we examined genes implicated in regulating cardiac trabeculation and ventricular compaction. We found that the basic cell-cycle regulators cyclin D1 and c-Myc were highly expressed in the ventricular myocardium of $Gbe^{-/-}$ embryos compared with that of WT embryos. Although the details of the molecular mechanisms responsible for cardiomyocyte hyperproliferation have not been fully examined, our findings provide a starting point for further investigation. Furthermore, the possibility that physiologic and molecular changes in other organs (e.g. liver secretion of growth factors) could lead to secondary changes in the hearts of $Gbe1^{-/-}$ mice also needs to be further investigated.

In summary, using a gene-driven ENU-mutagenesis approach, we have generated a Gbe1-deficient mouse model that recapitulates the clinical features of hydrops fetalis and the embryonic lethality of severe fetal forms of GSD-IV. Contrary to expectations, $Gbe^{-/-}$ embryos showed less glycogen accumulation than their WT littermates, little amylopectin accumulation and no evidence of cell degeneration. Our data indicate that, in addition to the deposition of amylopectin-like polysaccharides, which presumably leads to cell death in the tissues, a novel mechanism leading to uncontrolled cardiomyocyte proliferation and trabeculation/compaction of the ventricular wall contributes to abnormal cardiac development and fetal hydrops in GSD-IV. Further studies on the mechanisms that control cardiomyocytes proliferation/maturation can be expected to enhance our ability to repair heart injury in adults and induce cardiac regeneration.

MATERIALS AND METHODS

Screening for *Gbe1* mutations and generation of $Gbe^{-/-}$ mice

ENU mutagenesis, screening of mutation-bearing mice and *in vitro* fertilization for mutant mice generation were performed by Ingenium Pharmaceuticals, Germany (17). Briefly, C3HeB/FeJ male mice were treated with ENU. Genomic DNA from G1 male mice was archived for mutation

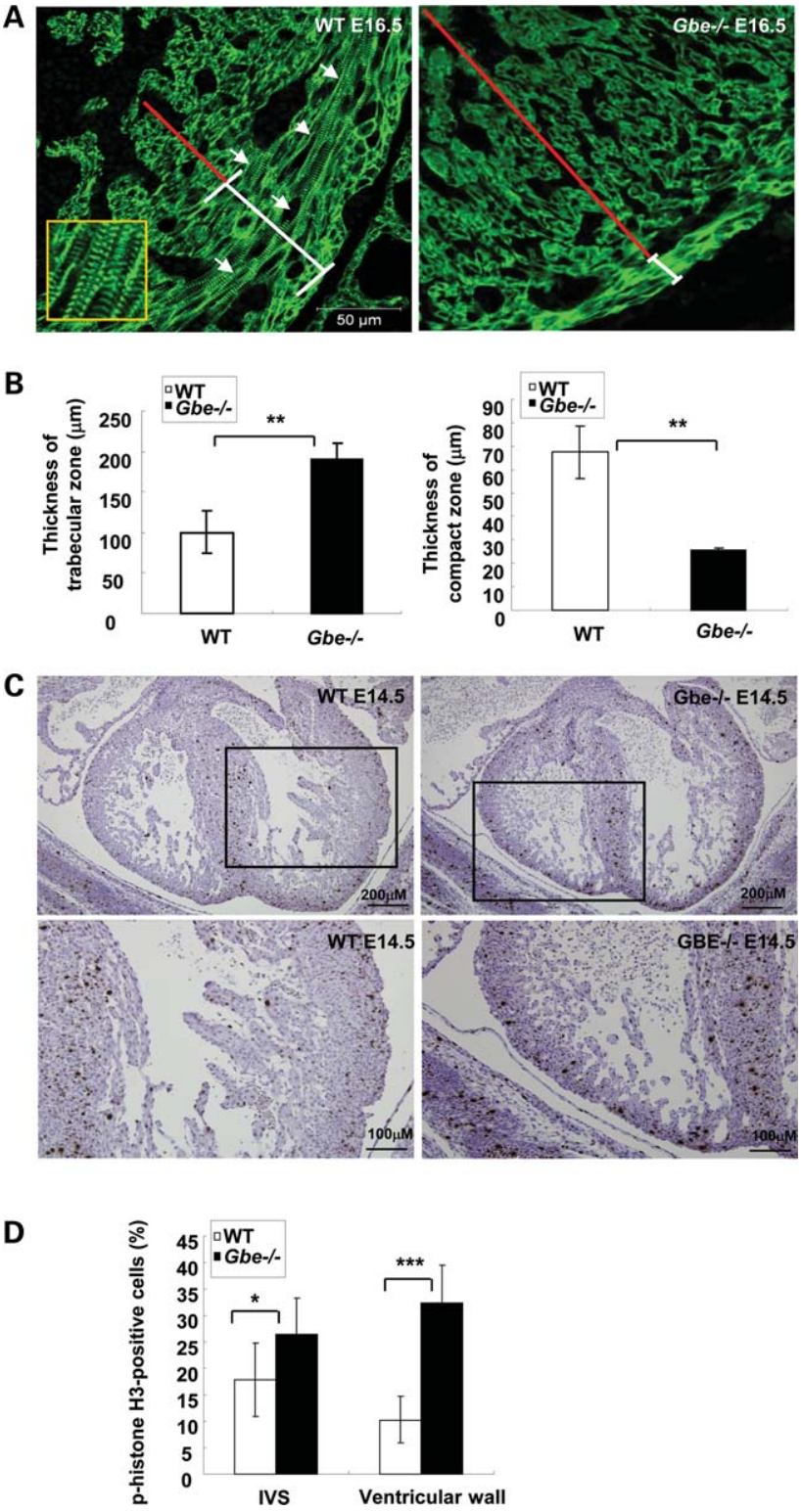

Figure 5. Hypertrabeculation and noncompaction in heart ventricles of late-gestation $Gbe^{-/-}$ embryos caused by hyperproliferation of cardiomyocytes. (**A**) Cardiomyocytes in the hearts of WT and $Gbe^{-/-}$ E16.5 embryos were identified using the myocardial marker MF-20. Images were acquired using a confocal microscope. Hypertrabeculation, noncompaction and thin ventricular walls are evident in $Gbe^{-/-}$ hearts. The red lines indicate the trabeculation regions, and the white lines show the compaction regions of the ventricular wall. A significant Z-line/body (arrows and inset), indicating the presence of well-organized sarcomeres, was observed in the hearts of E16.5 WT but not in the hearts of E16.5 $Gbe^{-/-}$. Scale bars: 50 μm. (**B**) Left panel: quantification of the thickness of the trabecular zone in $Gbe^{-/-}$ and WT hearts at E16.5 ($n = 3$ biological samples); right panel: quantification of the thickness of the compact zone in $Gbe^{-/-}$ and WT hearts at E16.5 ($n = 3$ biological samples). (**C**) Proliferating cells in the hearts of WT and $Gbe^{-/-}$ E14.5 embryos identified by staining for phosphorylated histone H3. Sections were stained with an anti-phospho-histone H3 antibody. Scale bars: 200 μm (upper panel) and 100 μm (lower panel). (**D**) Percentage of phospho-histone H3-positive cells at E14.5 in the interventricular septum region (IVS) and ventricular wall in $Gbe^{-/-}$ and WT hearts ($n = 3$ biological samples). The percentage of proliferating cardiomyocytes in $Gbe^{-/-}$ hearts was increased significantly.

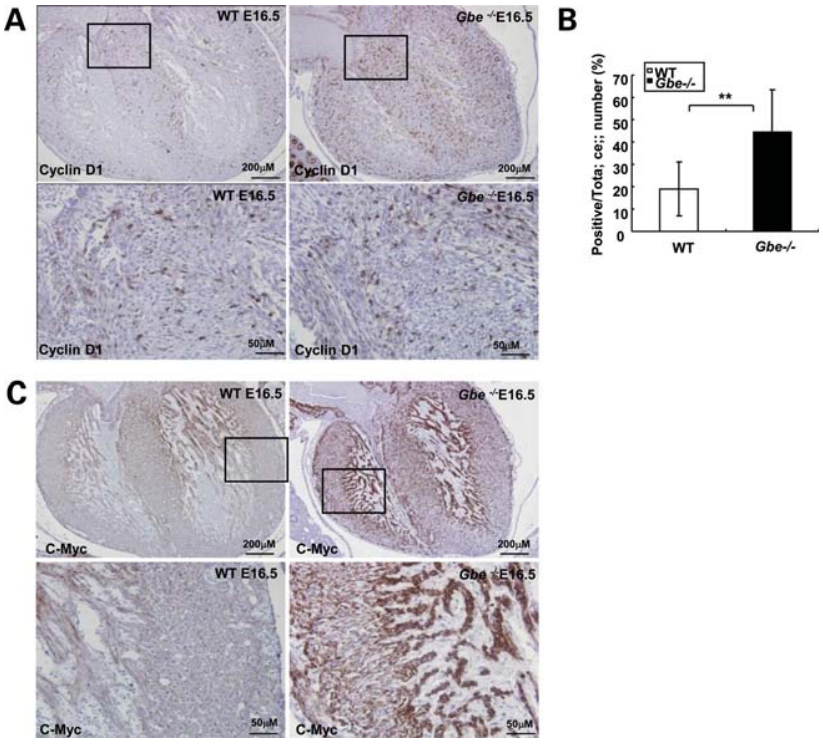

Figure 6. Cyclin D1 and c-Myc expression in the hearts of $Gbe^{-/-}$ and WT embryos. (**A**) Increased cyclin D1 in the hearts of $Gbe^{-/-}$ embryos. Sections were stained with anti-cyclin D1 antibody (brown) and then counterstained with hematoxylin to identify nuclei (blue). Note the overall increase in cyclin D1 staining in E16.5 $Gbe^{-/-}$ hearts. Scale bars: 200 μm (upper panel) and 50 μm (lower panel). (**B**) Percentage of cyclin D1-positive cells at E16.5 in the interventricular septum region and ventricular wall in $Gbe^{-/-}$ and WT embryonic hearts ($n = 3$ biological samples). (**C**) Increased c-Myc in the hearts of $Gbe^{-/-}$ E16.5 embryos. Sections were stained with anti-c-Myc antibody (brown) and then counterstained with hematoxylin to identify nuclei (blue). Note the overall increase in c-Myc staining in $Gbe^{-/-}$ hearts compared with WT hearts, where staining was restricted to a small area of trabecular myocardium. Scale bars: 200 μm (upper panel) and 50 μm (lower panel). The higher magnification images in (B) and (D) are demarcated in lower magnification panels.

screening, and the corresponding sperm samples were frozen for recovery of mutant mice. The mutations of interest in the collected DNA archives were screened by temperature-gradient capillary electrophoresis, and mutant lines (G2 generation) were established by *in vitro* fertilization using the banked sperm. After receiving the mice in our animal facility, G2 mice were outcrossed with WT C3HeB/FeJ for two more generations, and G4 heterozygous mice were intercrossed to generate homozygous mice. Mice were housed in a temperature- and humidity-controlled room with a 12 h light/12 h dark cycle under specific pathogen-free conditions. All animal protocols were approved by the institutional animal safety committee.

PCR and DNA sequencing

Genomic DNA from mice and developing embryos was prepared from tail and yolk sac, respectively. GeneBank accession number NT_039625 was used as the reference sequence for the mouse *Gbe1* gene. Mutations were genotyped by PCR amplification and sequencing. The sequences of the primers used for PCR amplification and DNA sequencing were 5′-AAA CTG TAG AGC TCA GAG ATT CCA-3′ (forward) and 5′-CAT CTT AAT AGG CAC ATG CAC TG-3′ (reverse).

Assessment of embryonic heart rate by ultrasound biomicroscopy Doppler

Embryonic Doppler echocardiography was performed noninvasively from day 10.5 to 19.5 post-coitum (E10.5–E19.5). After removing abdominal hair, the pregnant female was allowed to inhale 2% isoflurane and was then intubated via a nose cone with 1–1.5% isoflurane to maintain anesthesia. The mice were kept warm by placing on a heated platform, and body temperature and electrocardiograms were continuously monitored. For heart rhythm assessment, fetal heart images and blood velocities were obtained using a Vevo 660 scanner equipped with a 30 MHz ultrasound probe (VisualSonics, Inc., Ontario, Canada).

RNA isolation and quantitative real-time RT-PCR analysis

Total RNA from the hearts of various gestational age embryos was isolated using the TRIzol reagent (Invitrogen, Taipei, Taiwan) and further purified using an RNeasy Mini Kit (QIAGEN, Hilden, Germany). RNA was then treated with DNAse I (30 U/μg total RNA; QIAGEN) and reverse-transcribed using the SuperScript III First-Strand Synthesis System (Invitrogen). Expression of Gbe1 mRNA was quantified using SYBR Green PCR Master Mix and the ABI Prism 7900HT Sequence Detection System (Applied Biosystems,

Taipei, Taiwan). Gbe1 expression data were normalized to β-actin mRNA levels and presented as fold changes. The regions used to design *Gbe1* primers are indicated in Figure 2C. The primers used for amplifying β-actin mRNA were 5′-GGA CTC CTA TGT GGG TGA CG-3′ (forward) and 5′-CTT CTC CAT GTC GTC CCA GT-3′ (reverse). Primers for amplifying Bmp10 were 5′-ACA TCA TCC GGA GCT TCA AGA ACG-3 (forward) and 5′-AAC CGC AGT TCA GCC ATG ACG-3′ (reverse).

Histological analysis of embryos and mouse tissues

Embryos collected from timed heterozygous matings were immediately submerged in 3.6% neutral buffered paraformaldehyde solution and stored at 4°C until embedding in paraffin wax by standard methods. Placental tissue was collected for genotyping. The sections were stained with hematoxylin–eosin (H&E) or PAS (with or without pretreatment with diastase) by standard methods.

Determination of glycogen content

Glycogen content was estimated by measuring glucose released by Glycogen Assay Kit (BioVision, CA, USA), as described by the manufacturer. Briefly, glycogen was hydrolyzed with glycogen hydrolysis enzyme released by the kit, and the glycogen content was determined as glucose units analyzed colorimetrically with appropriate standard curve. The fresh samples were used for the determination, and the glucose background in the samples was also determined and subtracted from the glycogen content.

Immunohistochemical and immunofluorescence staining

For immunohistochemical staining of phosphorylated histone H3, cyclin D1 and c-Myc, paraffin-embedded sections were treated with 0.3% H_2O_2 and incubated with anti-phospho-histone H3 (1:200; Cell Signaling), anti-cyclin D1 (1:100; Epitomics, Inc., CA, USA) and anti-c-Myc (1:50; Epitomics, Inc.) antibodies, respectively. After incubation, the slides were washed and further incubated with a biotinylated secondary antibody (1:200; Vector Laboratories) for 1 h. Signals (brown) were detected using an avidin–biotin complex assay following the manufacturer's protocol (Vector Laboratories). Sections were counterstained with hematoxylin to identify nuclei (blue) and visualized by standard light microscopy. For immunofluorescence staining, paraffin-embedded heart sections were stained with a monoclonal anti-MF-20 antibody (1:500; Developmental Studies Hybridoma Bank, IA, USA). The signals were then detected with a fluorescein isothiocyanate-conjugated secondary antibody. Images were acquired using a Zeiss LSM 510 laser confocal microscope (Carl Zeiss MicroImaging, Inc., Hamburg, Germany).

Statistical analyses

A two-tailed Student's *t*-test was used to test for differences between treatments. A P–value <0.05 was considered statistically significant ($^{*}P$-value <0.05, $^{**}P$-value <0.01, $^{***}P$-value <0.001).

SUPPLEMENTARY MATERIAL

Supplementary Material is available at *HMG* online.

ACKNOWLEDGEMENTS

We acknowledge the Mouse Clinic Core, National Science Council, Taiwan, for technical help with mouse *in vivo* ultrasound biomicroscopy studies.

Conflict of Interest statement. None declared.

FUNDING

This work was supported by grants from the National Research Program for Genomic Medicine, Taiwan (National Genotyping Core, NSC- 98-3112-B-001-002) and Academia Sinica Genomic Medicine Multicenter Study, Taiwan (5202401129-3).

REFERENCES

1. Moses, S.W. and Parvari, R. (2002) The variable presentations of glycogen storage disease type IV: a review of clinical, enzymatic and molecular studies. *Curr. Mol. Med.*, **2**, 177–188.
2. Brown, B.I. and Brown, D.H. (1966) Lack of an alpha-1,4-glucan: alpha-1,4-glucan 6-glycosyl transferase in a case of type IV glycogenosis. *Proc. Natl Acad. Sci. USA*, **56**, 725–729.
3. Servidei, S. and DiMauro, S. (1989) Disorders of glycogen metabolism of muscle. *Neurol. Clin.*, **7**, 159–178.
4. L'Hermine-Coulomb, A., Beuzen, F., Bouvier, R., Rolland, M.O., Froissart, R., Menez, F., Audibert, F. and Labrune, P. (2005) Fetal type IV glycogen storage disease: clinical, enzymatic, and genetic data of a pure muscular form with variable and early antenatal manifestations in the same family. *Am. J. Med. Genet. A,* **139A**, 118–122.
5. Cox, P.M., Brueton, L.A., Murphy, K.W., Worthington, V.C., Bjelogrlic, P., Lazda, E.J., Sabire, N.J. and Sewry, C.A. (1999) Early-onset fetal hydrops and muscle degeneration in siblings due to a novel variant of type IV glycogenosis. *Am. J. Med. Genet.*, **86**, 187–193.
6. van Noort, G., Straks, W., Van Diggelen, O.P. and Hennekam, R.C. (1993) A congenital variant of glycogenosis type IV. *Pediatr. Pathol.*, **13**, 685–698.
7. Tang, T.T., Segura, A.D., Chen, Y.T., Ricci, L.M., Franciosi, R.A., Splaingard, M.L. and Lubinsky, M.S. (1994) Neonatal hypotonia and cardiomyopathy secondary to type IV glycogenosis. *Acta Neuropathol.*, **87**, 531–536.
8. Herrick, M.K., Twiss, J.L., Vladutiu, G.D., Glasscock, G.F. and Horoupian, D.S. (1994) Concomitant branching enzyme and phosphorylase deficiencies. An unusual glycogenosis with extensive neuronal polyglucosan storage. *J. Neuropathol. Exp. Neurol.*, **53**, 239–246.
9. Reusche, E., Aksu, F., Goebel, H.H., Shin, Y.S., Yokota, T. and Reichmann, H. (1992) A mild juvenile variant of type IV glycogenosis. *Brain Dev.*, **14**, 36–43.
10. Schroder, J.M., May, R., Shin, Y.S., Sigmund, M. and Nase-Huppmeier, S. (1993) Juvenile hereditary polyglucosan body disease with complete branching enzyme deficiency (type IV glycogenosis). *Acta Neuropathol.*, **85**, 419–430.
11. Lossos, A., Barash, V., Soffer, D., Argov, Z., Gomori, M., Ben-Nariah, Z., Abramsky, O. and Steiner, I. (1991) Hereditary branching enzyme dysfunction in adult polyglucosan body disease: a possible metabolic cause in two patients. *Ann. Neurol.*, **30**, 655–662.

12. Bruno, C., Servidei, S., Shanske, S., Karpati, G., Carpenter, S., McKee, D., Barohn, R.J., Hirano, M., Rifai, Z. and DiMauro, S. (1993) Glycogen branching enzyme deficiency in adult polyglucosan body disease. *Ann. Neurol.*, **33**, 88–93.
13. Bao, Y., Kishnani, P., Wu, J.Y. and Chen, Y.T. (1996) Hepatic and neuromuscular forms of glycogen storage disease type IV caused by mutations in the same glycogen-branching enzyme gene. *J. Clin. Invest.*, **97**, 941–948.
14. Valberg, S.J., Ward, T.L., Rush, B., Kinde, H., Hiraragi, H., Nahey, D., Fyfe, J. and Mickelson, J.R. (2001) Glycogen branching enzyme deficiency in quarter horse foals. *J. Vet. Intern. Med.*, **15**, 572–580.
15. Fyfe, J.C., Kurzhals, R.L., Hawkins, M.G., Wang, P., Yuhki, N., Giger, U., Van Winkle, T.J., Haskins, M.E., Patterson, D.F. and Henthorn, P.S. (2007) A complex rearrangement in GBE1 causes both perinatal hypoglycemic collapse and late-juvenile-onset neuromuscular degeneration in glycogen storage disease type IV of Norwegian forest cats. *Mol. Genet. Metab.*, **90**, 383–392.
16. Bruno, C., van Diggelen, O.P., Cassandrini, D., Gimpelev, M., Giuffre, B., Donati, M.A., Introvini, P., Alegria, A., Assereto, S., Morandi, L. *et al.* (2004) Clinical and genetic heterogeneity of branching enzyme deficiency (glycogenosis type IV). *Neurology*, **63**, 1053–1058.
17. Augustin, M., Sedlmeier, R., Peters, T., Huffstadt, U., Kochmann, E., Simon, D., Schoniger, M., Garke-Mayerthaler, S., Laufs, J., Mayhaus, M. *et al.* (2005) Efficient and fast targeted production of murine models based on ENU mutagenesis. *Mamm. Genome*, **16**, 405–413.
18. Pashmforoush, M., Lu, J.T., Chen, H., Amand, T.S., Kondo, R., Pradervand, S., Evans, S.M., Clark, B., Feramisco, J.R., Giles, W. *et al.* (2004) Nkx2–5 pathways and congenital heart disease; loss of ventricular myocyte lineage specification leads to progressive cardiomyopathy and complete heart block. *Cell*, **117**, 373–386.
19. Chen, H., Zhang, W., Li, D., Cordes, T.M., Mark Payne, R. and Shou, W. (2009) Analysis of ventricular hypertrabeculation and noncompaction using genetically engineered mouse models. *Pediatr. Cardiol.*, **30**, 626–634.
20. Kerkela, R., Kockeritz, L., Macaulay, K., Zhou, J., Doble, B.W., Beahm, C., Greytak, S., Woulfe, K., Trivedi, C.M., Woodgett, J.R. *et al.* (2008) Deletion of GSK-3beta in mice leads to hypertrophic cardiomyopathy secondary to cardiomyoblast hyperproliferation. *J. Clin. Invest.*, **118**, 3609–3618.
21. Alegria, A., Martins, E., Dias, M., Cunha, A., Cardoso, M.L. and Maire, I. (1999) Glycogen storage disease type IV presenting as hydrops fetalis. *J. Inherit. Metab. Dis.*, **22**, 330–332.
22. Nambu, M., Kawabe, K., Fukuda, T., Okuno, T.B., Ohta, S., Nonaka, I., Sugie, H. and Nishino, I. (2003) A neonatal form of glycogen storage disease type IV. *Neurology*, **61**, 392–394.
23. Navaratnam, V. (1987) *Heart Muscle: Ultrastructural Studies*. Cambridge University Press, Cambridge.
24. Bhavnani, B.R. (1983) Ontogeny of some enzymes of glycogen metabolism in rabbit fetal heart, lungs, and liver. *Can. J. Biochem. Cell Biol.*, **61**, 191–197.
25. Dawes, G.S., Mott, J.C. and Shelley, H.J. (1959) The importance of cardiac glycogen for the maintenance of life in foetal lambs and newborn animals during anoxia. *J. Physiol.*, **146**, 516–538.
26. Gutierrez-Correa, J., Hod, M., Passoneau, J.V. and Freinkel, N. (1991) Glycogen and enzymes of glycogen metabolism in rat embryos and fetal organs. *Biol. Neonate*, **59**, 294–302.
27. Pederson, B.A., Chen, H., Schroeder, J.M., Shou, W., DePaoli-Roach, A.A. and Roach, P.J. (2004) Abnormal cardiac development in the absence of heart glycogen. *Mol. Cell Biol.*, **24**, 7179–7187.
28. Kaslow, H.R. and Lesikar, D.D. (1984) Isozymes of glycogen synthase. *FEBS Lett.*, **172**, 294–298.